Stochastic threshold in cell size control

Liang Luo [1,*,†] Yang Bai [2,*] and Xiongfei Fu [2,‡]

[1]*Department of Physics, Huazhong Agricultural University, Wuhan 430070, China*

[2]*CAS Key Laboratory for Quantitative Engineering Biology, Guangdong Provincial Key Laboratory of Synthetic Genomics, Shenzhen Institute of Synthetic Biology, Shenzhen Institutes of Advanced Technology, Chinese Academy of Sciences, Shenzhen 518055, China*

(Received 5 March 2022; accepted 22 February 2023; published 13 March 2023)

Classic models of cell size control consider that cells divide when reaching a threshold, e.g., size, age, or size extension. The molecular basis of the threshold involves multiple layers of regulation as well as gene noise. In this paper, we study the cell cycle as a first-passage problem with a stochastic threshold and discover that such stochasticity affects the intergeneration statistics, which bewilders the criteria to distinguish the types of size control models. The analytic results show that the autocorrelation in the threshold can drive a sizer model to the adderlike and even timerlike intergeneration statistics, which is supported by simulations. Following the picture that the autocorrelation in the threshold can propagate to the intergeneration statistics, we further show that the adder model can be driven to the timerlike one by a positively autocorrelated threshold, and even to the sizerlike one when the threshold is negatively autocorrelated. This work highlights the importance of examining gene noise in size control.

DOI: 10.1103/PhysRevResearch.5.013173

I. INTRODUCTION

Cell size homeostasis requires microbes to tightly control the fluctuations in exponential size growth and cell division [1,2]. The mechanism of cell size control has been a puzzle for half a century since the discovery of the cell growth law by Schaechter, Maaløe, and Kjeldgaard [3]. Modern experiments integrating the techniques of microfluidics and advanced imaging analysis shed light on the puzzle, which allows direct measurements of cell cycles in a branch of the lineage [4]. The size control dynamics have been investigated since then in the phenomenological styles [5–10], focusing on the intergeneration series of birth size x_b, division size x_d, and intergeneration time τ. According to the intergeneration correlations, the experimental data are classified into three types as follows: the sizer, wherein the division size x_d is independent of the birth size x_b; the adder, wherein the size extension $\Delta = x_d - x_b$ is independent of x_b; and the timer, wherein τ is independent of x_b. Concerning the underlying mechanisms of the classes, three types of models have been proposed [1,11–13], assuming that cell division happens when a certain accumulating division indicator reaches a characteristic threshold. Different indicators are assumed for different types of intergeneration correlation, which could be the cell size for the "sizer," the added size since birth for the adder, and the cell age since birth for the timer [5,14–16], where the simplified principle can be hence summarized by Figs. 1(a) and 1(b).

The intergeneration correlations have been important criteria for biologists to search for the signal molecule that regulates cell division [1]. Since the adder correlation is widely reported by experiments for bacteria such as *Escherichia coli* [1,15,17–19], the indicator of size extension has been intensively investigated [18,20–26]. An attractive mechanism arises from the previous studies that the formation of the division ring plays a key role in communicating cell mass accumulation and cell division. The accumulation of the related FtsZ protein then becomes a strong candidate as the indicator of size extension [18,23,24,26]. The accumulation mechanics of the adder mechanism hence draws attention from the theoretical side [27–33], while experiments searching for the molecular mechanics of cell size control are still in progress.

Recent experiments reported conflicting data that the statistics shifts from the adderlike correlation to the sizerlike one in the slow-growth condition [7,29,34]. The correlation as a mixture of adder and sizer seems to be demanding more complicated regulatory mechanisms. There have been candidates: Mixed models have been proposed in which the DNA replication initiates with the sizer or adder control mechanism while the replication requires roughly constant time [18,20,22,34]. Concurrent models state that the cell divides only when both indicators reach the threshold [25,26,35]. Models based on the dynamics of biochemical reactions also seem to work [8,28,32]. All of the models respect the principle of the correspondence between the indicator and the intergeneration correlation. It is, however, not necessarily true. In the recent study by Berger and ten Wolde [36], it was discovered that a

*These authors contributed equally to this work.
†Corresponding author: luoliang@mail.hzau.edu.cn
‡Corresponding author: xiongfei.fu@siat.ac.cn

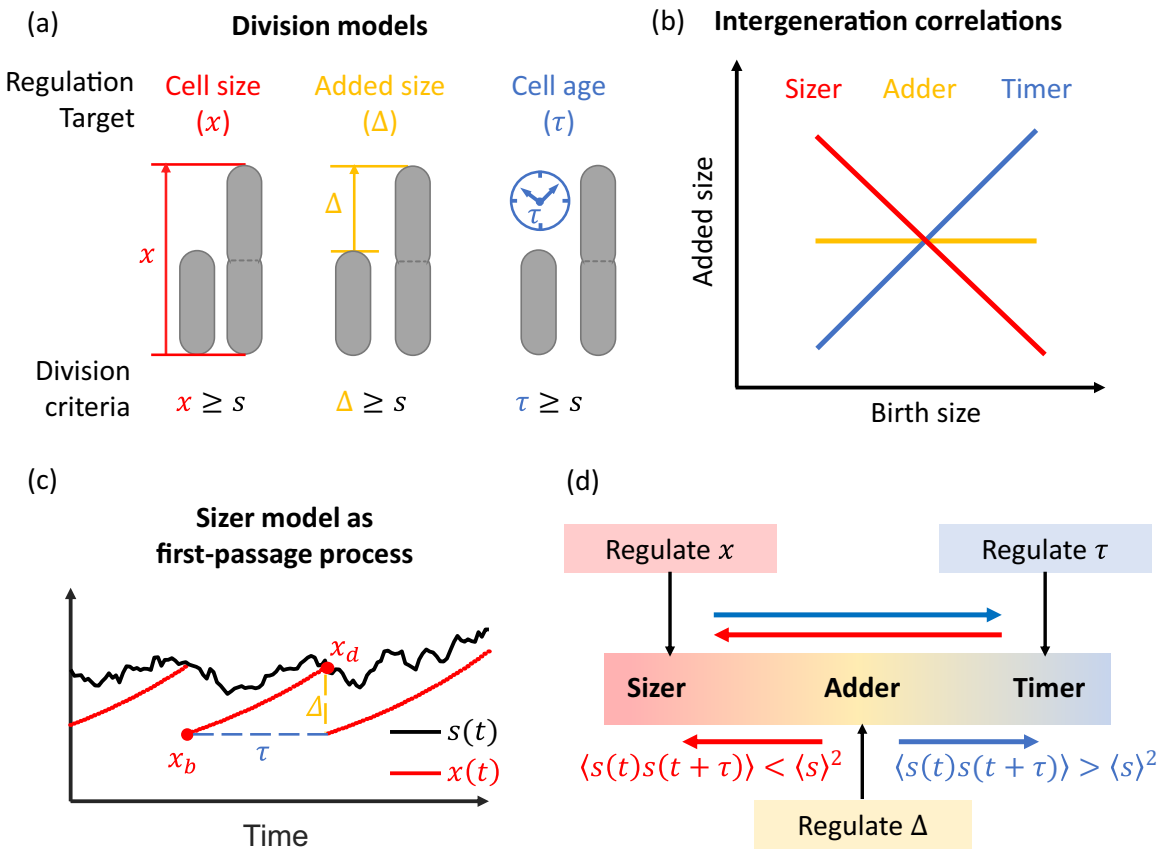

FIG. 1. The intergeneration correlation observed in experiments reflects both the regulatory mechanism and the correlation in the stochastic threshold. The three mechanisms with cell size, size extension, and cell age as the cell cycle indicator [see (a)] led to the native intergeneration correlation as sizer, adder, and timer [see (b)]. The accumulation model describes the cell cycles as the first-passage process, as illustrated in (c) with sizer mechanism as an example. The birth size x_b, the division size x_d, the added size Δ, and the intergeneration time (or generation time) τ are depicted. (d) The autocorrelation of the stochastic threshold $s(t)$ could drive the intergeneration correlation either from sizer to adder to timer [with positive autocorrelation, i.e., $\langle s(t)s(t+\tau)\rangle - \langle s\rangle^2 > 0$] or the reverse [with negative autocorrelation, i.e., $\langle s(t)s(t+\tau)\rangle - \langle s\rangle^2 < 0$].

sizer model can also have an adderlike intergeneration correlation in the case of a fluctuating threshold.

We realize that the molecular determinants of the division threshold would be involved in complex regulatory networks, e.g., DNA replication, divisome formation, or mass accumulation [23,24,34]. Imposed on noise in the regulatory networks, the division threshold would surely follow a certain stochastic process, in which not only the magnitude of fluctuation but also the autocorrelation matters. The autocorrelation in the stochastic threshold may thus propagate into the intergeneration correlation, which breaks the principle of the correspondence between the indicator and the intergeneration correlation. This paper aims to clearly demonstrate that the hidden correlation in the stochastic threshold would lead to a significant shift of the observed intergeneration correlation, which can be dramatically different from the native one.

In this paper, a first-passage framework for the cell cycle is developed, which includes all three regulatory mechanisms. We analytically demonstrate that the mechanism with cell size as division indicator would lead to the adderlike and even timerlike intergeneration correlation, due to the autocorrelated stochastic threshold $s(t)$. In the case of limited statistics, as is usual in experiment, the adderlike state can hardly be distinguished from that from the native mechanism with added size as the indicator. We then demonstrate that the mechanism regulating the added size would be driven to the timerlike one by positively correlated $s(t)$, and even back to the sizerlike one by the negatively correlated $s(t)$. This allows a continuous shift from adderlike to sizerlike correlation in slow-growth conditions, which has been reported in recent experiments. A comprehensive picture is hence created showing how the autocorrelation in the threshold modifies the intergeneration correlation type.

II. THEORETICAL FRAMEWORK FOR BACTERIAL CELL CYCLES

In this section, we introduce the theoretical framework for the dynamics of bacterial cell cycles, which has been established in the recent decade [5,6,27,31,37]. The main idea is that the dynamics can be decomposed into two processes of different scales. On the single-cell scale, the intrageneration

process focuses on the dynamics from cell birth to cell division. On the population scale, the intergeneration process can be modeled as a random walk of the birth size x_b over the generations (or the division size x_d, the generation time τ). The two processes are bridged by the propagator of the cell state from the mother of generation i to the daughter of generation $i+1$, which can be written as the conditional probability density $P(x_b^{(i+1)}, \tau | x_b^{(i)})$, assuming that the cell state can be well characterized by the birth size alone. The feature of the propagator has been the center of the previous investigations, either on the connection between the propagator and the time series observed in experiments [5,10], or on the theoretical constraints on the propagator [6]. Aiming to build a bridge from the intracellular dynamics to the intergeneration statistics, the propagators are constructed for various cell size control mechanisms [27,31,38], in which studies cell cycles are solved as first-passage processes to a certain threshold for cell division, which threshold has been simply assumed as a fixed value. The assumption would be inadequate, concerning the molecular basis of biological processes. The abundance of proteins, including the key ones controlling division threshold, generally fluctuate and are usually autocorrelated in a certain time scale. We extend here the first-passage framework for the cell cycle [31] to the case of a fluctuating and autocorrelated division threshold. The intergeneration propagator is obtained from the intracellular dynamics in this framework.

The intrageneration processes under various size control mechanisms can be included in the accumulation model. The model assumes that the cell accumulates a certain material as the index of its growth. The cell divides when the index reaches the fluctuating threshold s controlled around the expected value s_0, which dynamics can be written in the fashion of the Langevin equation as

$$\frac{ds}{dt} = g(s) + \eta_s, \tag{1}$$

where the function $g(s)$ controls the dynamics of s and η_s is the noise term. The sizer mechanism can be described by setting the index as the exponentially growing cell size x [36,38], i.e.,

$$\frac{dx}{dt} = \lambda x + \eta_x, \tag{2}$$

with the initial size $x(t=0) = x_b^{(i)}$. The cell divides once its size x reaches the size threshold s. The birth size of the daughter cell can be linked to the division size x_d by the distribution $P(x_b^{(i+1)} | x_d^{(i)})$. For the reader's intuition, the model is illustrated in Fig. 1(c). We assume perfect even division in this paper for simplicity, by directly setting $x_b^{(i+1)} = x_d^{(i)}/2$. Generalization to cases of uneven division [30,39] would be straightforward.

The adder mechanism can be similarly embraced in the accumulation model [27,31] by including the additional dynamics of the adder index u. The index increases with the exponential cell growth but is set to zero at birth as

$$\frac{du}{dt} = \frac{\lambda}{x_0} x + \eta_u, \tag{3}$$

where $u(t=0) = 0$. The cell divides when the index u reaches the threshold s for the first time. Assuming that s fluctuates around $s_0 = 1$, the parameter x_0 gives the expected added size in each cell cycle.

The timer mechanism can be modeled by setting the index as the cell age τ, which is of course set to zero at birth and linearly increases in the time course, $d\tau/dt = 1$. The cell divides when the age τ reaches the threshold s for the first time. It has been acknowledged that this control mechanism is not stable in the case of exponentially growing cell size [1,13].

Figure 1(a) illustrates the three mechanisms. Previous analysis suggests that the three mechanisms lead to different correlations between the birth size and the size extension over the cell cycle [1,13], as shown in Fig. 1(b). Let us refer to the correlations as "sizerlike," "adderlike," and "timerlike" ones in this paper.

In the above accumulation model, the cell cycle is formulated as the first-passage process (FPP) to the threshold. Due to the additional ending condition, the FPP is in general a more difficult problem than the original stochastic process. In the framework of the Fokker-Planck equation concerning the evolution of the probability density function $P(x, u, s, t)$, the ending condition can be translated as the absorbing boundary [31,40,41]. Let us consider the sizer mechanism as an example. In the Langevin form, it is given by Eqs. (1) and (2) with the first-passage condition $x = s$. Assuming white noise, the equivalent Fokker-Planck counterpart is written as

$$\frac{\partial P}{\partial t} = -\frac{\partial}{\partial x}(\lambda x P) + D_x \frac{\partial^2 P}{\partial x^2} - \frac{\partial}{\partial s}(g(s)P) + D_s \frac{\partial^2 P}{\partial s^2}. \tag{4}$$

The second-order diffusion terms are from the noise. D_x and D_s are the corresponding diffusion coefficients. For a cell with birth size x_b and known threshold value s_b, the initial condition is written as

$$P(x, s, t=0 | x_b, s_b) = \delta(x - x_b)\delta(s - s_b). \tag{5}$$

The first-passage condition is set by the absorbing (Dirichlet) boundary condition

$$P(x, s, t | x_b, s_b)|_\Omega = 0, \tag{6}$$

where the boundary $\Omega = \{(x, s) | x = s\}$. As the cell grows, the probability current is absorbed by the boundary. The survival probability can be introduced as

$$S(t | x_b, s_b) = \iint_{s>x} dx\, ds\, P(x, s, t | x_b, s_b), \tag{7}$$

where the initial condition with the birth size and the initial value of s is emphasized and the integration is over the region constrained by the boundary Ω. It gives the probability that the cell has not divided till time t, which probability constantly decreases from the initial value $S(t=0) = 1$. The first-passage time distribution can be evaluated as

$$F(t | x_b, s_b) = -\frac{\partial S(t | x_b, s_b)}{\partial t}. \tag{8}$$

In the language of the cell cycle, Eq. (8) gives the distribution of the intergeneration time $P(\tau = t | x_b, s_b) = F(t | x_b, s_b)$ conditioned by the given x_b and s_b. Concerning also the division size, the joint distribution $P(x_d, \tau | x_b, s_b)$ is given by the probability current over the absorbing boundary

$$P(x_d, \tau | x_b, s_b) = \hat{W} P|_{x=x_d, s=x_d, t=\tau}, \tag{9}$$

where the operator $\hat{W} = \lambda x - D_x \partial/\partial x + g(s) - D_s \partial/\partial s$.

In principle, the solution $P(x, s, t)$ contains the full information of the FPP, from which one can evaluate all the distributions concerned. It is, however, nontrivial to obtain $P(x, s, t)$, since it constantly deforms around the absorbing boundary. To be precise, the dynamics of x and s are independent in the Fokker-Planck equation [Eq. (4)], while the absorbing boundary [Eq. (6)] introduces the coupling between the two processes. It is fortunate that the coupling can be ignored while the first-passage current is mostly contributed by the effect of cell growth. We note that the size x is expected to be increasing in exponential fashion, $x = x_b \exp(\lambda t) + x'$, where x' comes from the growth noise with zero mean. The problem can hence be translated as the first-passage process of the fluctuating x' and s to the moving boundary $\Omega' = \{(x', s)|s = x' + x_b \exp(\lambda t)\}$. The first-passage current hence has contributions from both the moving boundary and the diffusion of x' and s. We assume here that the former one dominates the problem and neglect the latter one. Translating the problem back to the growing x and the fixed boundary, this assumption neglects the deformation of $P(x, s, t)$ around the absorbing boundary. The survival probability equation (7) is approximated as

$$S(t|x_b, s_b) = \iint_{s>x} dx\, ds\, G(x, s, t|x_b, s_b), \tag{10}$$

where $G(x, s, t|x_b, s_b)$ is the solution of the Fokker-Planck equation (4) with the initial condition (5) but with no boundary constraint. It can be further decomposed as $G(x, s, t|x_b, s_b) = G^{(x)}(x, t|x_b)G^{(s)}(s, t|s_b)$, where

$$\frac{\partial G^{(x)}}{\partial t} = -\frac{\partial}{\partial x}(\lambda x G^{(x)}) + D_x \frac{\partial^2}{\partial x^2} G^{(x)}, \tag{11}$$

$$\frac{\partial G^{(s)}}{\partial t} = -\frac{\partial}{\partial x}(g(s) G^{(x)}) + D_s \frac{\partial^2}{\partial x^2} G^{(s)}, \tag{12}$$

with the initial condition $G^{(x)}(x, t = 0|x_b) = \delta(x - x_b)$ and $G^{(s)}(s, t = 0|s_b) = \delta(s - s_b)$. The dynamics of x and s are hence decoupled, which makes the following analytic solution possible. A similar treatment has also been applied by Redner for the first-passage process to a fast-moving cliff [40].

In principle, all the cellular processes are stochastic, including cell growth, index accumulation, and partition of cell division. Noise from these processes is surely important. For the clarity of the theory, this study focuses on the effects of autocorrelation in the stochastic threshold, while other noise is ignored. Other noise can be integrated in the theoretical framework in future studies, which would not harm the key insight of this paper. In this assumption, the cell cycle with the birth size x_b can be decomposed into the deterministic growth $x = x_b \exp(\lambda t)$ and the stochastic process of s following Eq. (12) with the free-boundary condition. The survival probability that a cell with the given birth size $x_b = s_b$ has not divided till time t can be expressed as

$$S(t|s_b) = \int_{s>x} ds\, G^{(s)}(s, t|s_b). \tag{13}$$

The first-passage time can then be evaluated as

$$F(t|s_b) = -\frac{\partial S(t|s_b)}{\partial t}. \tag{14}$$

Assuming perfect even division, $x_b = s_b/2$. The distribution of intergeneration time follows

$$P(\tau|x_b) = F(t = \tau|s_b = 2x_b). \tag{15}$$

Noting $x_d = x_b \exp(\lambda\tau)$ and $P(x_d|x_b)dx_d = P(\tau|x_b)d\tau$, the division size distribution can be expressed as

$$P(x_d|x_b) = \frac{1}{\lambda x_d} P\left(\tau = \frac{1}{\lambda} \ln \frac{x_d}{x_b}|x_b\right), \tag{16}$$

which gives the full information of the correlation between the birth size and the division size. The added size distribution can be written as

$$P(\Delta|x_b) = P(x_d = x_b + \Delta|x_b). \tag{17}$$

The joint probability would be convenient in comparison with the experimental data, which avoids the issue of insufficient sampling on extreme x_b. In the case of known steady distribution $P(x_b)$, it can be written as

$$P(\Delta, x_b) = P(\Delta|x_b)P(x_b). \tag{18}$$

As a first taste of the above framework, we consider the noise-free limit with the fixed size threshold $s(t) = s_0$. In this case,

$$G^{(s)}(s, t|s_b) = \delta(s - s_0), \tag{19}$$

where the Dirac delta is used. The survival probability

$$\begin{aligned} S(t|s_b) &= \int_{\frac{s_0}{2}e^{\lambda t}}^{\infty} ds\, \delta(s - s_0), \\ &= H\left(\frac{1}{\lambda} \ln 2 - t\right), \end{aligned} \tag{20}$$

where $H(x)$ is the Heaviside step function. It leads to

$$P(\tau|x_b) = \delta(\tau - \tau_c) \tag{21}$$

with the expected intergeneration time $\tau_c = \ln 2/\lambda$. The division size distribution follows as

$$P(x_d|x_b) = \frac{1}{\lambda x_d} \delta\left(\frac{1}{\lambda} \ln \frac{x_d}{2x_b}\right) = \delta(x_d - s_0), \tag{22}$$

where $x_b = s_0/2$ is applied. This is the typical behavior of a deterministic sizer.

III. SIZER MECHANISM WITH STOCHASTIC THRESHOLD

The stochastic size threshold $s(t)$ is in general controlled by certain feedback circuits around the mean value s_0. Let us consider the simplest case that $g(s) = -\gamma(s - s_0)$. We arrive at the Ornstein-Uhlenbeck (OU) process following the Fokker-Planck equation

$$\frac{\partial G^{(s)}}{\partial t} = \frac{\partial}{\partial s}(\gamma(s - s_0) G^{(s)}) + D \frac{\partial^2 G^{(s)}}{\partial s^2}. \tag{23}$$

The diffusion coefficient is simply marked as D since it is the only diffusion term. In the long-time limit, the stationary distribution follows the Gaussian style as

$$P_{st}(\tilde{s}) = \sqrt{\frac{1}{2\pi\sigma^2}} \exp\left[-\frac{\tilde{s}^2}{2\sigma^2}\right], \tag{24}$$

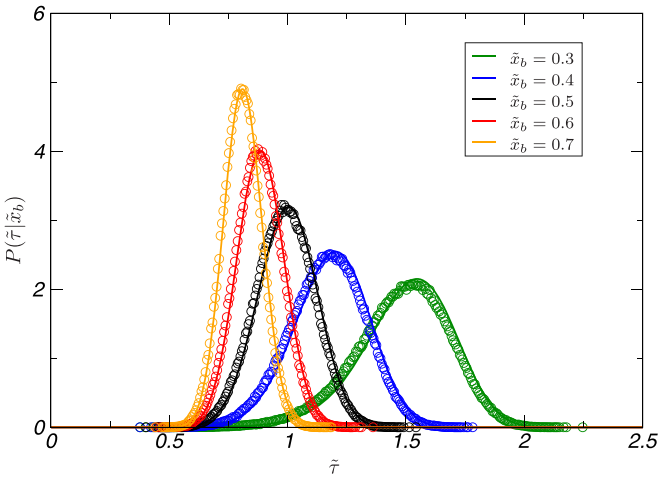

FIG. 2. The distribution of interdivision time $P(\tilde{\tau}|\tilde{x}_b)$ for the Ornstein-Uhlenbeck case with $\epsilon = 1$, $\sigma = 0.1$, and various birth sizes $\tilde{x}_b$. The solid lines are given by Eq. (27), and the symbols are from simulations.

where $\tilde{s} = s/s_0 - 1$, and the variance is controlled by the diffusion coefficient D as $\sigma^2 = D/(\gamma s_0^2)$. γ reflects the strength of the feedback control on s to the mean value s_0, which determines the typical correlation time as $t_c = 1/\gamma$. Introducing the rescaled time $\tilde{t} = t/t_c$, the Green's function of the Ornstein-Uhlenbeck process [42] can be written as

$$G^{(s)}(\tilde{s},\tilde{t}|\tilde{s}') = \left[\frac{1}{2\pi\sigma^2(1-e^{-2\tilde{t}})}\right]^{\frac{1}{2}} \exp\left[-\frac{(\tilde{s}-\tilde{s}'e^{-\tilde{t}})^2}{2\sigma^2(1-e^{-2\tilde{t}})}\right]. \tag{25}$$

One can see the OU process is positively correlated in the time scale of t_c. In the case that the generation time τ is also in this scale, the correlation can propagate into the intergeneration size correlation, which eventually changes the correlation classes.

The cell cycle is equivalent to the first-passage process of the fluctuating $\tilde{s}$ to a shifting absorbing boundary at $\tilde{x}(t) - 1$, where the exponentially growing size is rescaled by

$$\tilde{x}(t) = \frac{x_b}{s_0}\exp(\lambda t). \tag{26}$$

Equations (13)–(15) lead to the distribution of rescaled intergeneration time $\tilde{\tau} = \lambda\tau/\ln 2$ as

$$\begin{aligned} P(\tilde{\tau}|\tilde{x}_b) = &\left(\frac{1}{2\pi\sigma^2}\right)^{1/2}(1-e^{-2\tilde{\tau}})^{-3/2}[\epsilon\tilde{x}_b e^{\epsilon\tilde{\tau}}(1-e^{-2\tilde{\tau}}) \\ &+(1-\tilde{x}_b e^{\epsilon\tilde{\tau}})e^{-2\tilde{\tau}} - (1-2\tilde{x}_b)e^{-\tilde{\tau}}] \\ &\times \exp\left[-\frac{((1-2\tilde{x}_b)e^{-\tilde{\tau}} - (1-\tilde{x}_b e^{\epsilon\tilde{\tau}}))^2}{2\sigma^2(1-e^{-2\tilde{\tau}})}\right], \end{aligned} \tag{27}$$

where $\tilde{x}_b = x_b/s_0$. $\epsilon = \lambda/\gamma$ reflects the ratio of two key time scales, i.e., the expected intergeneration time τ_c and the typical correlation time t_c. Equation (27) has good agreement with the simulation, as shown in Fig. 2. This confirms the availability of the above approximation for this first-passage problem. One can further obtain the other distributions concerned. Let us consider the ratio $\alpha = \tilde{x}_d/\tilde{x}_b$, the distribution of which follows

$$\begin{aligned} P(\alpha|\tilde{x}_b) = &\left(\frac{1}{2\pi\sigma^2}\right)^{1/2}\frac{1}{\alpha\epsilon}(1-\alpha^{-2/\epsilon})^{-3/2}[\epsilon\alpha\tilde{x}_b(1-\alpha^{-2/\epsilon}) \\ &+(1-\alpha\tilde{x}_b)\alpha^{-2/\epsilon} - (1-2\tilde{x}_b)\alpha^{-1/\epsilon}] \\ &\times \exp\left[-\frac{(\alpha^{-1/\epsilon}(1-2\tilde{x}_b) - (1-\alpha\tilde{x}_b))^2}{2\sigma^2(1-\alpha^{-2/\epsilon})}\right]. \end{aligned} \tag{28}$$

In the $\epsilon \ll 1$ limit, $s(t)$ and $s(t+\tau_c)$ have little correlation because $\tau_c \gg t_c$. The above distribution turns into a Gaussian one as

$$P_{\epsilon\to 0}(\alpha|\tilde{x}_b) = \frac{1}{\sqrt{2\pi\sigma^2}}\tilde{x}_b \exp\left[-\frac{(\alpha\tilde{x}_b - 1)^2}{2\sigma^2}\right]. \tag{29}$$

Noting $x_d = \alpha s_0 \tilde{x}_b$, one can see that the division size fluctuates around s_0 with the distribution

$$P_{\epsilon\to 0}(x_d|x_b) = \frac{1}{\sqrt{2\pi\sigma^2 s_0^2}}\exp\left[-\frac{(x_d - s_0)^2}{2\sigma^2 s_0^2}\right]. \tag{30}$$

The variance is inherited from $s(t)$ as $\langle(x_d - s_0)^2\rangle = D/\gamma$. It is typical "sizer" behavior that the division size is governed by the threshold but independent of the birth size, as shown in Fig. 3(a) (see the line corresponding to $\epsilon = 0.1$).

In the $\epsilon \gg 1$ limit, $s(t)$ and $s(t+\tau_c)$ are strongly correlated. Equation (28) turns into

$$\begin{aligned} P_{\epsilon\to\infty}(\alpha|\tilde{x}_b) = &\sqrt{\frac{\epsilon\tilde{x}_b^2}{4\pi\sigma^2}}\frac{2-\alpha+2\alpha\ln\alpha}{2\alpha(\ln\alpha)^{3/2}} \\ &\times \exp\left[-\frac{\epsilon\tilde{x}_b^2(\alpha-2)^2}{4\sigma^2\ln\alpha}\right]. \end{aligned} \tag{31}$$

It is a distribution peaked around $\alpha = 2$ with the variance proportional to $\sigma^2/\epsilon x_b^2$. The division size x_d is always about twice the birth size x_b. The intergeneration time $\tau = \frac{1}{\lambda}\ln\alpha$ is largely independent of x_b, as shown on the right side of Fig. 3(c) (see the line corresponding to $\epsilon = 10$). In simple words, it behaves as a typical "timer." The above two limit cases can also be plotted as a usual practice on a diagram of $\Delta = x_d - x_b$ versus x_b, according to two straight lines with slope $k = -1$ (sizer correlation) and $k = 1$ (timer correlation), as shown by the $\epsilon = 0.1$ case and the $\epsilon = 10$ case in Fig. 3(b).

The crossover between the sizer and timer limits arises around $\epsilon \sim 1$, which behaves like the adder as shown below. For general ϵ, the full expressions of the distributions are rather complicated. The analytic estimation of the mean value is hard, if achievable. In the current case of small variance, one can turn to the mode of the distribution as an approximation. Take the division size $\tilde{x}_d$ as an example, the distribution of which can be obtained from Eq. (28) via the relation $\alpha = \tilde{x}_d/\tilde{x}_b$. We note that the peak of the distribution is governed by the factor

$$P(\tilde{x}_d|\tilde{x}_b) \propto \exp(-z^2/(2g\sigma^2)), \tag{32}$$

where $g = (\tilde{x}_d/\tilde{x}_b)^{2/\epsilon} - 1$ mainly modulates the peak width and $z = (2\tilde{x}_b - 1) + (\tilde{x}_d/\tilde{x}_b)^{1/\epsilon}(1 - \tilde{x}_d)$. Setting $z = 0$, one can estimate the position of the peak $\hat{x}_d$ by

$$(2\tilde{x}_b - 1) + (\hat{x}_d/\tilde{x}_b)^{1/\epsilon}(1 - \hat{x}_d) = 0. \tag{33}$$

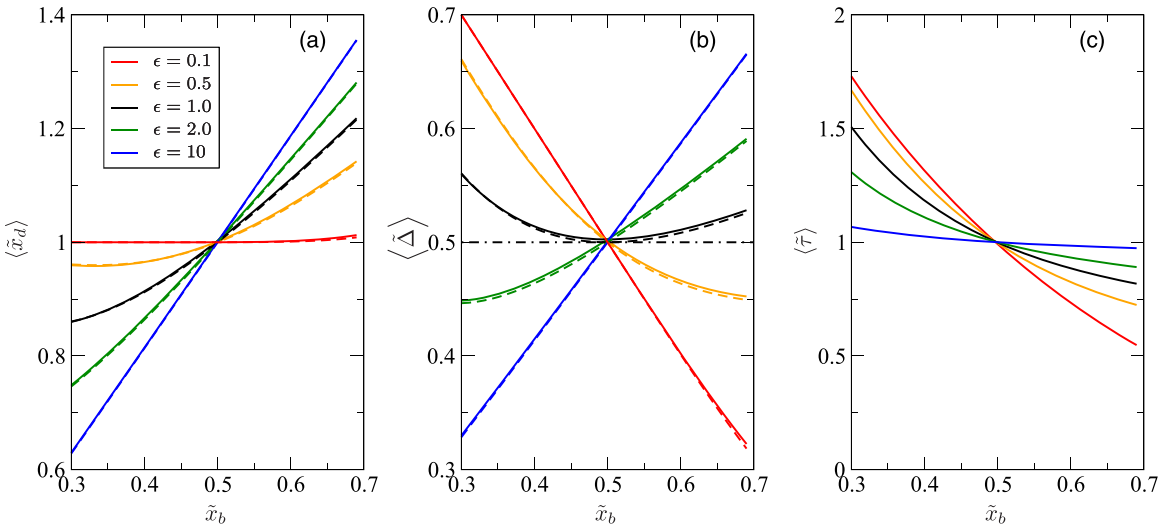

FIG. 3. The intergeneration correlation in the Ornstein-Uhlenbeck case. (a) The mean division size $\langle \tilde{x}_d \rangle$ conditioned by the given birth size $\tilde{x}_b$ for $\sigma = 0.1$ and various ϵ. The dashed lines show the typical value $\hat{x}_d$ solved from Eq. (33), which almost collapse to the mean values. (b) Same as (a), but for the mean added size $\langle \tilde{\Delta} \rangle$. The dash-dotted line shows the perfect adder correlation for guidance. (c) Same as (a), but for the mean intergeneration time $\langle \tilde{\tau} \rangle$.

In the $\epsilon \ll 1$ limit, the above equation is satisfied only if $2\tilde{x}_b - 1 = 0$ and $\hat{x}_d - 1 = 0$, which gives the sizer behavior shown above. In the $\epsilon \gg 1$ limit, Eq. (33) requires $\hat{x}_d = 2\tilde{x}_b$, which is the timer case discussed above. Concerning the relation between the typical added size $\hat{\Delta} \equiv \hat{x}_d - \tilde{x}_b$ and the birth size $\tilde{x}_b$, the crossover between the above two limits can be characterized by the slope $k \equiv d\hat{\Delta}/d\tilde{x}_b$. In the regime with which we are concerned around $\tilde{x}_b = 1/2$, Eq. (33) suggests

$$k = 2^{1-1/\epsilon} - 1, \tag{34}$$

which smoothly shifts from $k = -1$ for the $\epsilon \ll 1$ sizer limit to $k = 1$ for the $\epsilon \gg 1$ timer limit, as shown in Fig. 3(b). One may immediately note that $k = 0$ when $\epsilon = 1$. In this case, the typical added size $\hat{\Delta}$ gently depends on the birth size and slightly deviates from the expected value $1/2$, as shown in Fig. 3(b). The model hence behaves like the adder one, bearing small errors.

The reader may concern about the deviation of the $\epsilon = 1$ case from the perfect adder shown as the dash-dotted line in Fig. 3(b). However, the deviation can hardly be identified in experiments, where the statistics is commonly limited. To illustrate this, we performed a simulation with 10^4 cell cycles. Figure 4(a) shows the x_b-Δ scatterplot, which looks just like that of the adder model. The mean added size slightly deviates for the extreme birth sizes. However, the deviation might be ignored by the eye due to the poor statistics in these regions. The collapse of the added size distribution $P(\Delta|x_b)$ for various x_b is another key observation in experiments [15], which has been an important support to the accumulation mechanics [27,31]. In the current model, the distribution slightly changes for various birth sizes, but the distributions look very similar in the range $x_b/s_0 \approx 0.4$–0.6, where one can merely observe insignificant differences of peak heights, as shown in Fig. 4(b).

All of the above analysis is based on the model with $s(t)$ following the OU process. To confirm that the transition between the correlation types is induced by the autocorrelation in the threshold $s(t)$ but is not induced otherwise, we modified $s(t)$ from the OU process to a Gaussian-distributed random series. The positive autocorrelation is introduced into the series by a filter in Fourier space. The adderlike correlation arises again when the correlation time and the generation time match (not shown here).

In this section, we have demonstrated that the positive autocorrelation in the threshold can propagate into the intergeneration statistics, driving the sizer-type intergeneration correlation between size extension and birth size to an adderlike and even timerlike correlation. This can be the con-

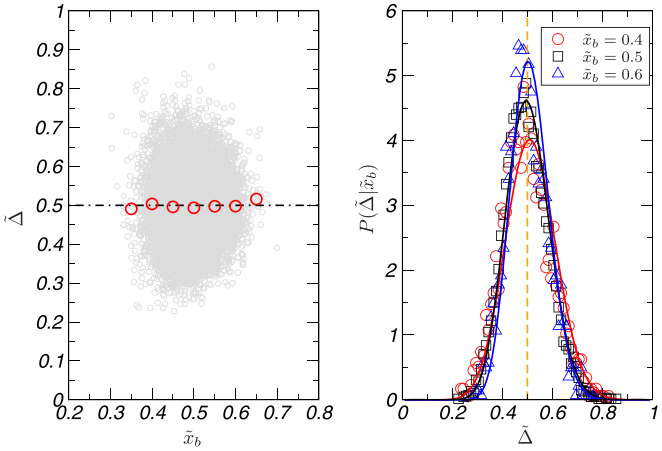

FIG. 4. The statistics of simulation of 10^4 cell cycles of the sizer mechanism with the threshold $s(t)$ following the OU process with $\epsilon = 1$, $s_0 = 1$, and $\sigma = 0.1$. (a) A scatterplot of the birth sizes vs the added sizes is shown by the gray circles. The mean added sizes for the given birth size are shown by the red circles. The black dash-dotted line indicates the added size for the perfect adder. (b) The distribution of the added size conditioned by various birth sizes, $P(\tilde{\Delta}|\tilde{x}_b)$ for $\epsilon = 1$ and $\sigma = 0.1$. The solid lines are the analytic results. The symbols are from the simulation.

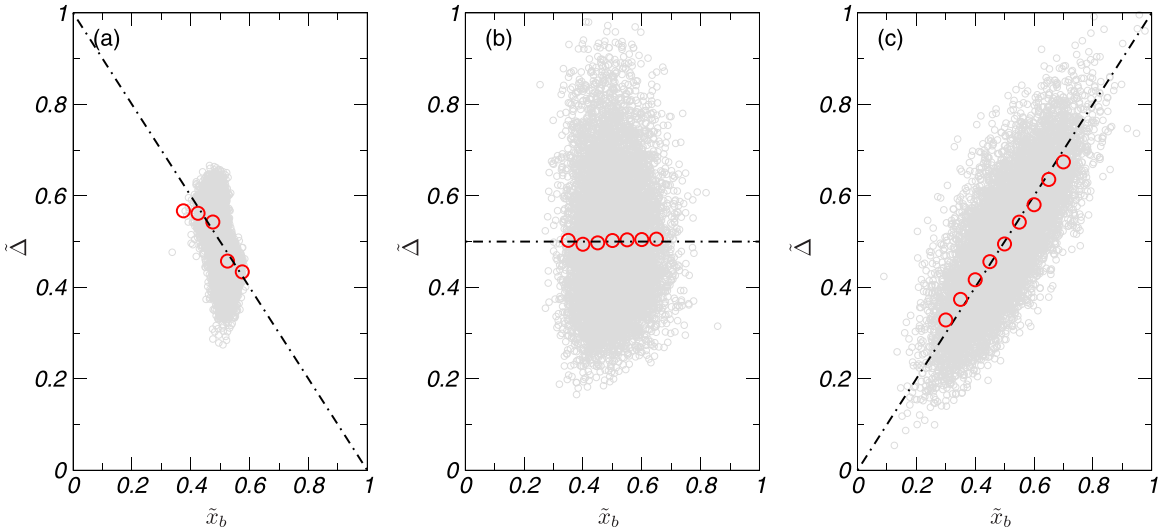

FIG. 5. The intrinsic correlation modifies the intergeneration correlation of the accumulator mechanics, shown by the x_b-Δ scatterplot of simulation data (gray circles). The red circles denote the mean added size $\langle\Delta\rangle$ for the given x_b. The dash-dotted lines show the perfect sizer, adder, and timer correlations for guidance. (a) The oscillating threshold $s(t)$ drives the native adder correlation to the sizerlike one when the oscillation period $T \simeq 2\tau_c$. (b) The native adder correlation of the accumulator with stochastic threshold $s(t)$ in the uncorrelated limit with $\epsilon = t_c \ln 2/\tau_c = 0.1$. (c) The positively correlated threshold $s(t)$ drives the native adder correlation to the timerlike one in the strong-correlation limit with $\epsilon = 10$.

sequence of a more general scheme. The observables, such as the division size, are sampled from a hidden stochastic process $s(t)$ by the time interval τ_c. The correlation of $s(t)$ may hence be inherited by the observables when τ_c is smaller than the correlation time of $s(t)$. This scheme can be generalized to the mechanism regulating other quantities, such as the added size shown in the next section.

IV. ADDER MECHANISM: THE EFFECTS OF POSITIVE CORRELATION AND NEGATIVE CORRELATION

The adder mechanism has been defined in Sec. II by introducing additional dynamics of the adder index u in Eq. (3). The cell divides when the adder index u reaches the threshold s for the first time. In the deterministic limit with $s = 1$, one can easily see that $x_d = x_b + x_0$. This is the native adder correlation of the adder mechanism. In the stochastic version ignoring the correlation in noise, the adder correlation is kept as shown in Fig. 5(b), as is well known in the literature. In the presence of the correlation in threshold s, the type of intergeneration correlation may be modified either to timerlike or to sizerlike.

To introduce the positive correlation, one can again assume s following the OU process with the intrinsic correlation time t_c. In the $t_c \gg \tau_c$ limit, $s(t)$ and $s(t + \tau_c)$ are strongly positively correlated. This modifies the type of intergeneration correlation towards the more positively correlated case, i.e., the timerlike correlation, as shown in Fig. 5(c). To drive an adder to the sizerlike one, the additional negative correlation is required.

We expect that negative autocorrelation in $s(t)$ would drive the adder mechanism to the sizerlike correlation. The negative correlation can arise in the oscillating threshold s. To be explicit, the autocorrelation of $s(t)$ and $s(t + \tau)$ is negative when the periods of the oscillator $T \simeq 2\tau_c$. In this paper, we have applied the oscillating dynamics of gene circuits given by Ref. [43] for demonstration. The dynamics considers the repressilator of three genes following

$$\frac{dm_i}{dt} = -m_i + \frac{\alpha}{1 + p_j^n} + \alpha_0,$$
$$\frac{dp_i}{dt} = -\beta(p_i - m_i), \tag{35}$$

where m_i is the mRNA concentration of gene i, p_i is the protein abundance in the cell, n is the Hill index, $i = 1, 2, 3$, and $j = \mathrm{mod}(i, 3) + 1$. In the unstable regime of the parameter space, the dynamics oscillates. Supposing an adder mechanism with the threshold controlled by such oscillating circuits, a negative correlation appears when the generation time is roughly half the period. The negative correlation propagates into the intergeneration size correlation via negatively regulated generation time. The cell sizes are hence more tightly controlled, leading to a sizerlike correlation shown in Fig. 5(a), where the randomness is introduced by the additional white noise on the threshold. In general, negative autocorrelation can arise from oscillating dynamics as long as the sampling interval is around half the period, $\tau \simeq T/2$. It is, however, sensitive to the noise in the threshold. Due to this concern, the simulation data shown in Fig. 5(a) are more compactly distributed, while the picture that the autocorrelation in the threshold modifies the intergeneration size correlation remains valid. We have also performed the simulation on the deterministic oscillating threshold and stochastic index accumulation. It is more robust to yield the sizerlike correlation, while the distributions look more similar to the experiment data. To avoid confusion and distraction, the results are not shown here. We would like to note that Berger and ten Wolde have discovered similar phenomena in their model (see Supplemental Material of Ref. [36]).

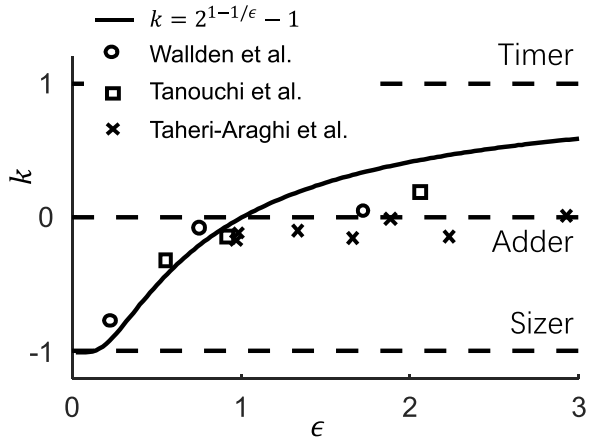

FIG. 6. The autocorrelation in the threshold modifies the intergeneration correlation of the sizer mechanism. The slope $k = d\Delta/dx_b$ as a function of $\epsilon = \lambda/\gamma = t_c \ln 2/\tau$. The symbols are from the experimental data of Tanouchi *et al.* [7], Taheri-Araghi *et al.* [15], and Wallden *et al.* [34], assuming $t_c = 1.2$ h. The black dashed lines show the perfect sizer, adder, and timer correlations for guidance.

V. DISCUSSION AND SUMMARY

This study represents a general picture of cell size control integrating randomness and autocorrelation in the stochastic threshold. It includes the naive deterministic model as the zero-noise limit, and the previously studied stochastic models as the uncorrelated limit. In the presence of gene noise and autocorrelation, we show that the positive autocorrelation in the stochastic threshold would drive the intergeneration size correlation, which has been the key observation in experiment, shifting smoothly from sizerlike to adderlike and then to timerlike, while the negative autocorrelation drives it in the reverse direction, as indicated by the arrows in Fig. 1(d).

The adderlike correlation appears in the sizer mechanism when the correlation time of the process, t_c, matches the generation time τ. When the two times differ, the correlation shifts to either the sizer or the timer one. The robust adder correlation is, however, observed in most experiments of fast-growth conditions, as shown by the symbols in Fig. 6. The question hence arises as to how the two time scales would match in these experiments. A conjecture follows. It has been noticed that the partition of cytoplasm in cell division is rather stochastic (see, e.g., Refs. [30,39]). The partition noise may disturb the hidden process $s(t)$ and shorten its correlation to the generation time τ. In simple words, t_c is capped by τ. The intergeneration correlation is hence locked in the adderlike one in fast-growth conditions. If this conjecture stands, one may expect in the slow-growth case that τ would be much longer than the intrinsic correlation time t_c and the cell size control would slip from the adder to the sizer. It is surprising to us that experiments [7,34] did observe the significant shift to sizerlike behavior in slow-growth cases, as shown in the region of $\epsilon < 1$ in Fig. 6.

Noting the shift between adderlike and sizerlike correlations, Tanouchi *et al.* [7] have proposed a phenomenological model by assuming the relation between the birth size and division size $x_d = ax_b + b + \eta$, where η is uncorrelated white noise. This kind of model [7,8] decomposes the randomness and the correlation into η and the slope a, which helps to capture the features of the experimental data. In the x_b vs Δ diagram, one can immediately read $a = k + 1$, which slope k is evaluated in this paper by Eq. (34). We noticed that the deviation from the adderlike correlation has also been investigated in the framework of the accumulation model since Ref. [27]. It was suggested that in the case where the division index is accumulated in the bursting style with the bursting size depending on the cell volume, the intergeneration correlation is more sizerlike. Nieto *et al.* [29] extended the accumulation model to the accumulation rate depending on the cell volume in a nonlinear way, which can also continuously bridge the sizerlike and adderlike behavior. In spite of the theoretical attempts, the reason for the shift between adder and sizer is still unclear. It may be a key to fully understanding the bacterial cell size control mechanism, which requires more hints from further experiments.

The recent wave of investigations on cell cycle control has largely been energized by modern techniques and experiments, which directly observe the cell cycles on the single-cell level. On the cell level, the phenomenological models are promising for consistent description of the observation. The biologists may go further, asking about the biological mechanism behind the phenomenological model. The accumulation model [27,29,31] has been utilized in this paper to build a bridge from the phenomenological description to its physical basis, i.e., the accumulation of a certain index. Although we still have no definitive answer on the molecular process, the accumulation models show more structures of the regulated cell cycles [27,31]. It is suggested that cell division is *not* a trivial Markovian process governed by a single rate, which leads to consequences on the population level [44,45]. It is also only in a model concerning more fundamental processes [36] that one may realize that the autocorrelation of the intracellular processes can propagate into the intergeneration observation, as also shown in this paper. The current study hence emphasizes the understanding of cell size control on the circuit level, in which direction there have been rapid advances [30,46–51].

Cellular noise is ubiquitous. Other stochastic processes (e.g., mass accumulation, uneven partition during division) would also contribute to the modification of intergeneration statistics [39]. We have already found the noise in accumulation would increase the variance of the birth size and the added size in the case of adder mechanics with oscillating threshold, yielding sizerlike correlation. It is worthwhile to further investigate the quantitative details of the models studied, such as the variance of the added size conditioned by the given birth size or other higher moments. Here, for simplicity, we only consider the influence of the noisy threshold to qualitatively illustrate the propagation of the correlation from intracellular process to intergeneration statistics.

Control of cell division and control of DNA replication are both important to a stable cell cycle. This paper focuses on the former one, while the latter one is surely interesting, even more crucial in the view from the biological side. The studies on the control of DNA replication also benefit from the mother machine experiments. The phenomenological description [18,26,34] has been obtained. The molecular basis was proposed even earlier. As a prominent example, the DNA

replication that determines the later cell division is initiated when cells reach a critical threshold of active DnaA protein [52]. Experimental evidence was reported for the possible regulation of active DnaA protein such as negative feedback of datA sites [53] or dnaA boxes [54], which could generate autocorrelated stochasticity in the threshold. The recent study by Berger and ten Wolde [36] was indeed aimed at a cell cycle model controlling DNA replication initiation, which leads to their observation of the emergence of adderlike correlation from a sizer controlling mechanism. The connection between the control of cell division and the control of DNA replication [18,23,26,35,55] is a matter of serious debate, which requires further investigation, especially from the experiment side.

In short summary, this study clearly shows how the autocorrelation of the intracellular process can modify the type of intergeneration correlation. As a consequence, the controlling mechanisms *cannot* be directly inferred from the intergeneration correlation. This calls for more careful inference based on the experimental observations. We highlight that simultaneous measurements of the intergeneration correlation and the stochasticity of the intracellular variables are important to validate the cell cycle control models.

ACKNOWLEDGMENTS

We thank C. Liu for the discussions. This work is partially supported by the National Key Research and Development Program of China (Grants No. 2018YFA0903400 and No. 2021YFA0910703), the Strategic Priority Research Program of Chinese Academy of Sciences (Grant No. XDB0480000), the NSFC (Grants No. 11705064 and No. 32071417), and Shenzhen Science and Technology Program (Grant No. ZDSYS20220606100606013).

[1] L. Willis and K. C. Huang, Sizing up the bacterial cell cycle, Nat. Rev. Microbiol. **15**, 606 (2017).

[2] S. Jun, F. Si, R. Pugatch, and M. Scott, Fundamental principles in bacterial physiology—history, recent progress, and the future with focus on cell size control: A review, Rep. Prog. Phys. **81**, 056601 (2018).

[3] M. Schaechter, O. Maaløe, and N. O. Kjeldgaard, Dependency on medium and temperature of cell size and Cchemical composition during balanced growth of *Salmonella typhimurium*, J. Gen. Microbiol. **19**, 592 (1958).

[4] P. Wang, L. Robert, J. Pelletier, W. L. Dang, F. Taddei, A. Wright, and S. Jun, Robust growth of *Escherichia coli*, Curr. Biol. **20**, 1099 (2010).

[5] A. Amir, Cell Size Regulation in Bacteria, Phys. Rev. Lett. **112**, 208102 (2014).

[6] J. Grilli, M. Osella, A. S. Kennard, and M. C. Lagomarsino, Relevant parameters in models of cell division control, Phys. Rev. E **95**, 032411 (2017).

[7] Y. Tanouchi, A. Pai, H. Park, S. Huang, R. Stamatov, N. E. Buchler, and L. You, A noisy linear map underlies oscillations in cell size and gene expression in bacteria, Nature (London) **523**, 357 (2015).

[8] L. Susman, M. Kohram, H. Vashistha, J. T. Nechleba, H. Salman, and N. Brenner, Individuality and slow dynamics in bacterial growth homeostasis, Proc. Natl. Acad. Sci. USA **115**, E5679 (2018).

[9] P. Thomas, Analysis of cell size homeostasis at the single-cell and population level, Front. Phys. **6**, 64 (2018).

[10] F. Jafarpour, Cell Size Regulation Induces Sustained Oscillations in the Population Growth Rate, Phys. Rev. Lett. **122**, 118101 (2019).

[11] L. Robert, Size sensors in bacteria, cell cycle control, and size control, Front. Microbiol. **6**, 515 (2015).

[12] G. Vuaridel-Thurre, A. R. Vuaridel, N. Dhar, and J. D. McKinney, Computational analysis of the mutual constraints between single-cell growth and division control models, Adv. Biosyst. **4**, 1900103 (2020).

[13] L. Olivi, M. Berger, R. N. P. Creyghton, N. De Franceschi, C. Dekker, B. M. Mulder, N. J. Claassens, P. R. ten Wolde, and J. van der Oost, Towards a synthetic cell cycle, Nat. Commun. **12**, 4531 (2021).

[14] W. J. Voorn, L. J. H. Koppes, and N. B. Grover, Mathematics of cell division in *Escherichia coli*: Comparison between sloppy-size and incremental-size kinetics, Curr. Top. Mol. Genet. **1**, 187 (1993).

[15] S. Taheri-Araghi, S. Bradde, J. T. Sauls, N. S. Hill, P. A. Levin, J. Paulsson, M. Vergassola, and S. Jun, Cell-size control and homeostasis in bacteria, Curr. Biol. **25**, 385 (2015).

[16] F. Si, D. Li, S. E. Cox, J. T. Sauls, O. Azizi, C. Sou, A. B. Schwartz, M. J. Erickstad, Y. Jun, X. Li, and S. Jun, Invariance of initiation mass and predictability of cell size in Escherichia coli, Curr. Biol. **27**, 1278 (2017).

[17] M. Campos, I. V. Surovtsev, S. Kato, A. Paintdakhi, B. Beltran, S. E. Ebmeier, and C. Jacobs-Wagner, A constant size extension drives bacterial cell size homeostasis, Cell **159**, 1433 (2014).

[18] G. Witz, E. van Nimwegen, and T. Julou, Initiation of chromosome replication controls both division and replication cycles in *E. coli* through a double-adder mechanism, eLife **8**, e48063 (2019).

[19] S. Bakshi, E. Leoncini, C. Baker, S. J. Cañas-Duarte, B. Okumus, and J. Paulsson, Tracking bacterial lineages in complex and dynamic environments with applications for growth control and persistence, Nat. Microbiol. **6**, 783 (2021).

[20] P.-Y. Ho and A. Amir, Simultaneous regulation of cell size and chromosome replication in bacteria, Front. Microbiol. **6**, 662 (2015).

[21] H. Zheng, P.-Y. Ho, M. Jiang, B. Tang, W. Liu, D. Li, X. Yu, N. E. Kleckner, A. Amir, and C. Liu, Interrogating the *Escherichiacoli* cell cycle by cell dimension perturbations, Proc. Natl. Acad. Sci. USA **113**, 15000 (2016).

[22] F. Barber, P.-Y. Ho, A. W. Murray, and A. Amir, Details matter: Noise and model structure set the relationship between cell size and cell cycle timing, Front. Cell Dev. Biol. **5**, 92 (2017).

[23] F. Si, G. Le Treut, J. T. Sauls, S. Vadia, P. A. Levin, and S. Jun, Mechanistic origin of cell-size control and homeostasis in bacteria, Curr. Biol. **29**, 1760 (2019).

[24] H. Zheng, Y. Bai, M. Jiang, T. A. Tokuyasu, X. Huang, F. Zhong, Y. Wu, X. Fu, N. Kleckner, T. Hwa, and C. Liu, General

quantitative relations linking cell growth and the cell cycle in Escherichia coli, Nat. Microbiol. **5**, 995 (2020).

[25] M. Panlilio, J. Grilli, G. Tallarico, I. Iuliani, B. Sclavi, P. Cicuta, and M. Cosentino Lagomarsino, Threshold accumulation of a constitutive protein explains *E. coli* cell-division behavior in nutrient upshifts, Proc. Natl. Acad. Sci. USA **118**, e2016391118 (2021).

[26] A. Colin, G. Micali, L. Faure, M. Cosentino Lagomarsino, and S. van Teeffelen, Two different cell-cycle processes determine the timing of cell division in *Escherichia coli*, eLife **10**, e67495 (2021).

[27] K. R. Ghusinga, C. A. Vargas-Garcia, and A. Singh, A mechanistic stochastic framework for regulating bacterial cell division, Sci. Rep. **6**, 30229 (2016).

[28] P. P. Pandey, H. Singh, and S. Jain, Exponential trajectories, cell size fluctuations, and the adder property in bacteria follow from simple chemical dynamics and division control, Phys. Rev. E **101**, 062406 (2020).

[29] C. Nieto, J. Arias-Castro, C. Sánchez, C. Vargas-García, and J. M. Pedraza, Unification of cell division control strategies through continuous rate models, Phys. Rev. E **101**, 022401 (2020).

[30] C. Jia and R. Grima, Frequency Domain Analysis of Fluctuations of mRNA and Protein Copy Numbers within a Cell Lineage: Theory and Experimental Validation, Phys. Rev. X **11**, 021032 (2021).

[31] L. Luo, Y. Bai, and X. Fu, Master equation approach to the stochastic accumulation dynamics of bacterial cell cycle, New J. Phys. **23**, 083029 (2021).

[32] L. Li, Balanced biosynthesis and trigger threshold resulting in a double adder mechanism of cell size control, Commun. Theor. Phys. **73**, 085601 (2021).

[33] A. Genthon, Analytical cell size distribution: Lineage-population bias and parameter inference, J. R. Soc. Interface **19**, 20220405 (2022).

[34] M. Wallden, D. Fange, E. G. Lundius, Ö. Baltekin, and J. Elf, The synchronization of replication and division cycles in individual *E. coli* cells, Cell **166**, 729 (2016).

[35] G. Micali, J. Grilli, M. Osella, and M. C. Lagomarsino, Concurrent processes set *E. coli* cell division, Sci. Adv. **4**, eaau3324 (2018).

[36] M. Berger and P. R. ten Wolde, Robust replication initiation from coupled homeostatic mechanisms, Nat. Commun. **13**, 6556 (2022).

[37] F. Jafarpour, C. S. Wright, H. Gudjonson, J. Riebling, E. Dawson, K. Lo, A. Fiebig, S. Crosson, A. R. Dinner, and S. Iyer-Biswas, Bridging the Timescales of Single-Cell and Population Dynamics, Phys. Rev. X **8**, 021007 (2018).

[38] S. Iyer-Biswas, G. E. Crooks, N. F. Scherer, and A. R. Dinner, Universality in Stochastic Exponential Growth, Phys. Rev. Lett. **113**, 028101 (2014).

[39] P. Thomas, G. Terradot, V. Danos, and A. Y. Weiße, Sources, propagation and consequences of stochasticity in cellular growth, Nat. Commun. **9**, 4528 (2018).

[40] S. Redner, *A Guide to First-Passage Processes* (Cambridge University Press, Cambridge, 2001).

[41] B. Qiu, T. Zhou, and J. Zhang, Stochastic fluctuations in apoptotic threshold of tumour cells can enhance apoptosis and combat fractional killing, R. Soc. Open Sci. **7**, 190462 (2020).

[42] H. Risken, *The Fokker-Planck Equation: Methods of Solution and Applications*, Springer Series in Synergetics Vol. 18 (Springer, New York, 1996).

[43] M. B. Elowitz and S. Leibler, A synthetic oscillatory network of transcriptional regulators, Nature (London) **403**, 335 (2000).

[44] F. Jafarpour, E. Levien, and A. Amir, Evolutionary dynamics in non-Markovian models of microbial populations, bioRxiv,.

[45] J. Zhang and T. Zhou, Markovian approaches to modeling intracellular reaction processes with molecular memory, Proc. Natl. Acad. Sci. USA **116**, 23542 (2019).

[46] D. Gomez, R. Marathe, V. Bierbaum, and S. Klumpp, Modeling stochastic gene expression in growing cells, J. Theor. Biol. **348**, 1 (2014).

[47] J. Lin and A. Amir, Homeostasis of protein and mRNA concentrations in growing cells, Nat. Commun. **9**, 4496 (2018).

[48] P. Thomas and V. Shahrezaei, Coordination of gene expression noise with cell size: Analytical results for agent-based models of growing cell populations, J. R. Soc. Interface **18**, 20210274 (2021).

[49] C. Jia, A. Singh, and R. Grima, Characterizing non-exponential growth and bimodal cell size distributions in fission yeast: An analytical approach, PLoS Comput. Biol. **18**, e1009793 (2022).

[50] C. Jia, A. Singh, and R. Grima, Concentration fluctuations in growing and dividing cells: Insights into the emergence of concentration homeostasis, PLoS Comput. Biol. **18**, e1010574 (2022).

[51] C. Jia and R. Grima, Coupling gene expression dynamics to cell size dynamics and cell cycle events: Exact and approximate solutions of the extended telegraph model, iScience **26**, 105746 (2023).

[52] D. P. Haeusser and P. A. Levin, The great divide: Coordinating cell cycle events during bacterial growth and division, Curr. Opin. Microbiol. **11**, 94 (2008).

[53] K. Kasho and T. Katayama, DnaA binding locus *datA* promotes DnaA-ATP hydrolysis to enable cell cycle-coordinated replication initiation, Proc. Natl. Acad. Sci. USA **110**, 936 (2013).

[54] F. G. Hansen, B. B. Christensen, and T. Atlung, Sequence characteristics required for cooperative binding and efficient *in vivo* titration of the replication initiator protein DnaA in *E. coli*, J. Mol. Biol. **367**, 942 (2007).

[55] G. L. Treut, F. Si, D. Li, and S. Jun, Quantitative examination of five stochastic cell-cycle and cell-size control models for *Escherichia coli* and *Bacillus subtilis*, Front. Microbiol. **12**, 721899 (2021).